  Bull. Chem. Soc. Jpn., 62, 1751—1757 (1989)

Relationships between Mesophase Behavior and Crystal Structures of Chiral Smectogenic 4-[(*S*)-2-Methylbutyl]phenyl 4′-Alkoxybiphenyl-4-carboxylates

Kayako Hori,* Miho Takamatsu, and Yuji Ohashi
Department of Chemistry, Ochanomizu University, Otsuka, Bunkyo-ku, Tokyo 112
(Received December 8, 1988)

Interlayer distances of Sm*C and Sm A phases of the title series were measured as functions of temperature by X-ray diffraction. With increase in temperature, molecular tilt angles in Sm*C decrease from 22—25 to 0°. Crystal structures of the heptyl (**1**) and octyl (**2**) homologues have been determined by X-ray analysis. (**1**): 4-[(*S*)-2-Methylbutyl]phenyl 4′-heptyloxybiphenyl-4-carboxylate, monoclinic, $P2_1$, a=26.929(4), b=5.4249(5), c=9.2607(9) Å, β=96.78(1)°, Z=2. (**2**): 4-[(*S*)-2-Methylbutyl]phenyl 4′-octyloxybiphenyl-4-carboxylate, orthorhombic, $P2_12_12_1$, a=9.249(1), b=56.259(9), c=5.412(1) Å, Z=4. Final R were 0.076 and 0.121, respectively. Both crystals have distinct layer structures similar to those of Sm*C. In the former crystal, the molecules tilt to one direction uniformly throughout layers, while in the latter, they take two opposite directions alternately from layer to layer. However, structures within a layer are very similar to each other. Each molecule has a coplanar biphenyl moiety and a twisted paraffin chain. Mesophase behavior was interpreted very well by the molecular interaction revealed in the crystal structures.

In the preceding paper,[1] we reported crystal structures of 4-pentyloxyphenyl and 4-heptyloxyphenyl 4′-[(*S*)-2-methylbutyl]biphenyl-4-carboxylates (series I crystals, abbreviated as I-5 and I-7, respectively) and discussed a relationship between the crystal structures and Sm*C phase characteristics. In order to make the relationship clearer, we extended the study to 4-[(*S*)-2-methylbutyl]phenyl 4′-alkoxybiphenyl-4-carboxylate series, $C_nH_{2n+1}O$-C_6H_4-C_6H_4-COO-C_6H_4-$CH_2CH(CH_3)C_2H_5$ (Series II, abbreviated as II-n), which is one of the isomeric series of the series I. While the series I has a Sm*C phase between crystalline and cholesteric phases, the series II has a Sm*C which transforms to a Sm A phase.[2] It has been pointed out that temperature dependence of the molecular tilt angles and behavior of transition to a higher temperature phase are different between the two kinds of Sm C, one which transforms to a nematic and the other to a Sm A.[3] This suggests different intermolecular interactions between the two Sm C. Therefore, it is considered to be very useful to find a relationship between crystal structures and mesophase behavior of the series II, and compare the relationship with that of the series I, in order to elucidate the intermolecular interaction.

This paper describes the mesophase behavior of the series II (n=6, 7, 8, 10, and 12) and the crystal structures of II-7 and II-8. Finally, relationships between the mesophase behavior and the crystal structures are discussed.

Experimental

Compounds. All the members were synthesized in a similar way to that described previously[4] from commercially available 4-alkoxy-4′-cyanobiphenyl (BDH Chemicals Ltd.) and 4-[(*S*)-2-methylbutyl]phenol supplied by BDH Chemicals Ltd., and purified by repeated crystallization from ethanol. All the crystalline samples thus obtained showed sharp melting (cryst-mesophase) peaks in the DSC measurements.

Studies of Mesophase Characteristics. Transition temperatures were measured using a Mettler TA 3000 DSC and an Olympus POM polarizing microscope equipped with a Mettler FP82. Interlayer distances were measured on a Rigaku 2001 diffractometer with Cu $K\alpha$ (λ=1.5418 Å) and Cr $K\alpha$ (λ=2.2902 Å). Helical pitches were measured as described previously.[4]

Crystal Structure Analysis. Transparent long parallelepiped crystals were grown from a methanol-chloroform solution. Crystals of approximate dimensions, 0.2×0.2×0.05 mm of II-7 and II-8 were used. The unit cell dimensions and space groups were determined from oscillation and Weissenberg photographs. Accurate cell parameters were determined by a least-squares fit for 15 reflections within the ranges $33°<2\theta<58°$ (II-7) and $37°<2\theta<50°$ (II-8), measured on a Rigaku AFC-4 diffractometer with Cu $K\alpha$ radiation (λ=1.54184 Å) monochromated by graphite.

Crystal Data. II-7, M_r=458.61, $C_{31}H_{38}O_3$, monoclinic, $P2_1$, a=26.929(4), b=5.4249(5), c=9.2607(9) Å, β=96.78(1)°, V=1343.4(3) Å^3, Z=2, d_x=1.134 g cm^{-3}, μ=4.84 cm^{-1}, $F(000)$=496; II-8, M_r=472.64, $C_{32}H_{40}O_3$, orthorhombic, $P2_12_12_1$, a=9.249(1), b=56.259(9), c=5.412(1) Å, V=2816(1) Å^3, Z=4, d_x=1.123 g cm^{-3}, μ=4.73 cm^{-1}, $F(000)$=1024. Reflection data were collected on a 2θ-ω scan mode, up to 2θ=125°, with scan widths of $\Delta\omega=(1.0+0.15\tan\theta)$ for II-7 and $\Delta\omega=(0.7+0.15\tan\theta)$ for II-8. Backgrounds were counted for 5 s at both ends of a scan. Three standard reflections were recorded after every 50 reflections. No significant intensity variations were observed. For II-7, a total of 2412 reflections were collected at the rate of 4° (2θ) min^{-1}, of which 1874 were treated as significant ($|F_o|>3\sigma(|F_o|)$). For II-8, 2691 reflections were collected at the rate of 4° (2θ) min^{-1}, of which 1540 were treated as significant. The data were corrected for Lorentz and polarization factors but not for absorption.

The structures were determined by applying the program MULTAN78[5] and refined by constrained block-matrix least-squares using SHELX76.[6] The quantity minimized

Table 1. Final Atomic Coordinates of II-7 with Their Estimated Standard Deviations, Multiplied by 10^4 for All the Atoms Except for C(25′) and 10^3 for C(25′)

Atom	x	y	z	B_{eq}/Å$^{2a)}$
O(1)	7116(2)	11163(12)	617(5)	7.1
O(2)	6857(1)	8063(9)	−864(4)	4.9
O(3)	3528(1)	8810(10)	4155(5)	5.8
C(1)	3991(2)	9016(10)	3711(5)	4.2
C(2)	4338(2)	10831(10)	4129(6)	5.2
C(3)	4795(2)	10864(11)	3583(7)	5.3
C(4)	4914(1)	9071(10)	2614(5)	4.0
C(5)	4562(2)	7213(11)	2208(6)	5.4
C(6)	4115(2)	7179(11)	2764(7)	5.2
C(7)	5411(1)	9159	1992(5)	3.5
C(8)	5764(2)	10955(12)	2444(7)	6.1
C(9)	6204(2)	11120(13)	1828(8)	6.7
C(10)	6316(2)	9435(10)	785(5)	4.1
C(11)	5972(2)	7576(11)	372(6)	5.2
C(12)	5530(2)	7440(10)	966(6)	5.0
C(13)	6800(2)	9649(13)	210(6)	4.5
C(14)	7324(2)	8017(11)	−1398(6)	4.9
C(15)	7453(2)	9841(11)	−2326(7)	5.4
C(16)	7916(2)	9797(12)	−2828(7)	5.9
C(17)	8246(2)	7877(12)	−2444(7)	5.6
C(18)	8109(2)	6011(12)	−1548(7)	6.1
C(19)	7649(2)	6102(11)	−1008(7)	5.5
C(21)	8754(2)	7884(21)	−3008(10)	6.9
C(22)	9124(3)	9786(21)	−2372(11)	8.3
C(23)	9600(4)	9690(33)	−3090(17)	12.3
C(24)	9916(7)	11966(39)	−2918(38)	20.3
C(25)$^{c)}$	9262(9)	8946(73)	−835(17)	20.5
C(31)	3370(2)	10606(15)	5113(7)	5.2
C(32)	2840(2)	9952(15)	5389(7)	5.0
C(33)	2686(3)	11526(18)	6618(9)	6.6
C(34)	2130(2)	11513(17)	6757(10)	7.3
C(35)	1905(3)	8978(19)	6910(10)	7.8
C(36)	1366(3)	9222(23)	7236(14)	10.0
C(37)	1122(4)	6756(27)	7407(20)	15.0
C(25′)$^{c)}$	949(4)	930(40)	−73(15)	29.7$^{b)}$

a) $B_{eq}=(4/3)\sum_{ij}\beta_{ij}(a_i\cdot a_j)$. b) Isotropic temperature factor. c) Occupation factors are fixed as 0.7 and 0.3 for C(25) and C(25′), respectively.

Table 2. Final Atomic Coordinates of II-8 with Their Estimated Standard Deviations, Multiplied by 10^4 for x and y, and 10^3 for z Coordinates

Atom	x	y	z	B_{eq}/Å$^{2a)}$
O(1)	7560(8)	8996(2)	648(2)	8.2
O(2)	8960(9)	9119(1)	345(2)	6.3
O(3)	2854(8)	10704(1)	424(2)	7.1
C(1)	3440(11)	10483(2)	442(2)	5.2
C(2)	3147(15)	10325(2)	632(2)	6.9
C(3)	3839(12)	10106(2)	622(2)	6.0
C(4)	4844(10)	10043(2)	443(2)	5.9
C(5)	5046(14)	10207(2)	249(2)	6.9
C(6)	4426(13)	10431(2)	257(2)	6.6
C(7)	5634(11)	9810(2)	458(2)	4.8
C(8)	5234(16)	9643(2)	633(3)	7.9
C(9)	6028(15)	9433(2)	643(3)	9.3
C(10)	7128(9)	9375(2)	479(2)	4.5
C(11)	7431(14)	9538(2)	294(2)	5.3
C(12)	6741(12)	9756(2)	288(2)	5.7
C(13)	7874(15)	9150(2)	509(2)	5.7
C(14)	9650(11)	8896(2)	344(2)	5.6
C(15)	9370(11)	8752(2)	143(2)	7.0
C(16)	10028(14)	8529(2)	128(2)	7.1
C(17)	10994(12)	8457(2)	307(2)	6.7
C(18)	11326(11)	8608(2)	504(2)	6.6
C(19)	10639(12)	8825(2)	524(2)	6.6
C(21)	11747(15)	8221(2)	311(3)	8.5
C(22)	11118(15)	8039(2)	491(3)	11.2
C(23)	11950(23)	7806(3)	469(4)	14.2
C(24)	11721(41)	7658(4)	694(6)	23.9
C(25)	9555(15)	7999(3)	434(5)	14.7
C(31)	1780(13)	10782(2)	604(3)	6.6
C(32)	1402(12)	11027(2)	542(3)	6.5
C(33)	71(14)	11105(2)	686(3)	7.4
C(34)	−142(19)	11369(2)	709(3)	10.3
C(35)	−463(18)	11486(2)	463(4)	12.9
C(36)	−1058(31)	11734(3)	505(5)	19.7
C(37)	−733(54)	11899(3)	295(5)	23.7
C(38)	−983(36)	12156(2)	367(7)	21.1

a) $B_{eq}=(4/3)\sum_{ij}\beta_{ij}(a_i\cdot a_j)$.

was $\sum w(|F_o|-|F_c|)^2$, where $w=(\sigma(F_o)^2+0.004|F_o|^2)^{-1}$. Atomic scattering factors were taken from the International Tables for X-ray Crystallography.[7] All the non-hydrogen atoms except for the disordered C(25′) atom of II-7 were refined anisotropically. Hydrogen atoms found in the difference Fourier maps and derived geometrically were refined isotropically. Max. Δ/σ and max. $\Delta\rho$ in the final difference map were 0.21 and 0.15 e Å^{-3} for II-7, and 0.45 and 0.27 e Å^{-3} for II-8. Final R (and R_w) were 0.076 (0.090) and 0.121 (0.141) for II-7 and II-8, respectively. Considerably large R value for II-8 is due to somewhat poor crystallinity. In spite of the repeated attempts of crystallization, the best crystal still showed broad rocking-curve along the ω direction. Data collected by ω-scan mode did not improve the ratio, $|F_o|/\sigma(|F_o|)$ and hence the final R-value, probably because of the wide-based peaks. The final coordinates of non-hydrogen atoms are given in Tables 1 (II-7) and 2 (II-8).[8] Computations were carried out on a HITAC M-280H computer at the Computer Center of the University of Tokyo.

Results

Phase Sequences. In order to discuss a relationship between a crystal structure and mesophase behavior, it is necessary to know to which mesophase the crystal transforms. While the series I has a relatively simple phase sequence, cryst.-Sm*C-chol.-isotropic, the series II was reported to have more complicated ones depending on the paraffin chain lengths and thermal history.[2] For example, it was reported that II-8 exhibits a phase sequence, cryst.-Sm*I-Sm*C Sm A-chol.-iso., while the II-7 crystal transforms directly to Sm*C. Besides, as supercooled phases, Sm*K and Sm*J for II-8 and Sm*K, Sm*J, and Sm*I for II-7 were reported. In the present DSC measurements, mesophase-mesophase or mesophase-isotropic transition temperatures were in good agreement with those reported for all the members, while cryst.-mesophase transition behavior for some members were slightly different from the reported one. For II-8, a solid sample obtained from a melt showed a complex curve corresponding to the reported supercooled

phase sequence, while the crystals obtained from a solution showed a simple and sharp melting curve similar to that of II-7, as shown in Fig. 1. This indicates that the crystal structures determined in this work transform directly to Sm*C. The enthalpy changes are 24.5 kJ mol^{-1} (II-7) and 25.5 kJ mol^{-1} (II-8).

Interlayer Distances and Helical Pitches in the Mesophase. Figure 2 shows the temperature dependence of the interlayer distances, d, in Sm*C and Sm A phases. The bending points are Sm*C-Sm A phase transition points. With increase in temperature, the d-values increase rapidly near the Sm*C-Sm A transition point in the Sm*C phase, while they decrease slightly in Sm A. Similar rapid dependence was observed for Sm C of 4′-octyloxybiphenyl-4-carboxylic acid[9] and attributed to the change of the molecular tilt angle in the Sm C phase. Figure 3 shows the relationship of the d-values at the transition points with the chain lengths, n. Good linearlity is obtained except for the member n=6 at the solid-Sm*C transition point. This exception is due to the extremely narrow temperature range for this member. Applying the equation, $d=d_r+n\times d_m$, to each line, the contribution to the layer thickness per methylene group, d_m, is obtained to be 0.90 (at the solid or other Sm-Sm*C), 0.77 (at Sm*C-Sm A) and 0.75 Å (at Sm A-chol. or isotropic transition point), showing that the contribution of the paraffin chain to the interlayer distances decreases slightly with increase in temperature throughout the two phases. On the other hand, the d_r value, i.e., that of the rest moiety of the molecule involving the core part and the bulky 2-methylbutyl group, is estimated to be 20.2 (at the solid or other Sm-Sm*C), 24.1 (at Sm*C-Sm A), and 23.9 Å (at Sm A-chol. or isotropic transition point). The latter two values are almost the same and attributed to the value for a molecule oriented vertically, on average, to the layer plane.

The tilt angle is estimated for each member, assuming that the layer thickness change is only due to the change of the average tilt angle of a whole molecule, since the change of the interlayer distances due to the

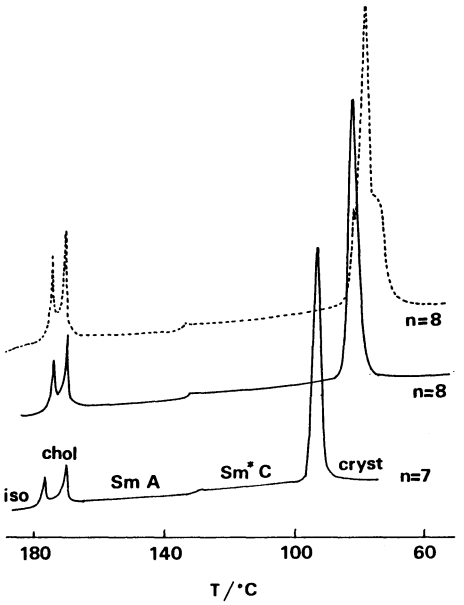

Fig. 1. DSC curves of 4-[(*S*)-2-methylbutyl]phenyl 4′-heptyloxybiphenyl-4-carboxylate (II-7) and 4-[(*S*)-2-methylbutyl]phenyl 4′-octyloxybiphenyl-4-carboxylate (II-8). A broken line denotes a curve for the solid of II-8 obtained from a melt. For II-7, DSC curves were almost independent of thermal history.

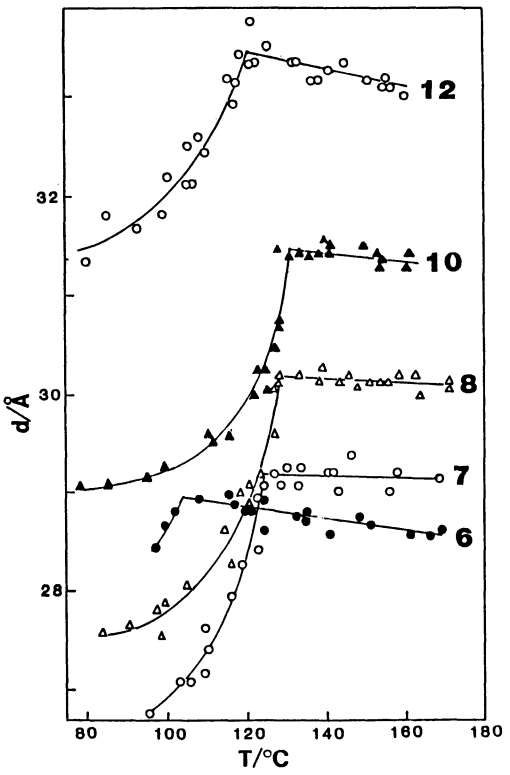

Fig. 2. Temperature dependence of interlayer distances of II-n (n=6, 7, 8, 10, and 12).

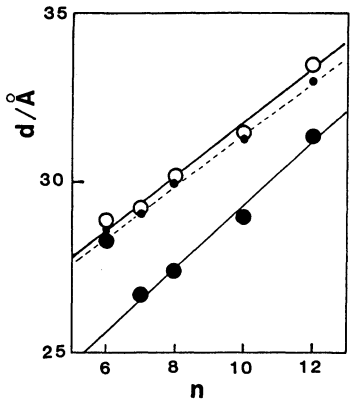

Fig. 3. Dependence of interlayer distances on the chain lengths. Open, filled (large), and filled (small) circles denote the d-values at solid (or Sm)-Sm*C, Sm*C-Sm A, and Sm A-chol. (or iso.), respectively.

paraffin chain is small, as mentioned above. The results are shown in Fig. 4. For the members with sufficiently wide temperature range of Sm*C, tilt angles are estimated to vary from 22—25 to 0° (assumed) with increase in temperature, approximately in accordance with a relation, $\theta \propto (T_c - T)^{\alpha}$, where T_c is Sm*C-Sm A transition temperature and α is estimated from the slope of relatively linear portions of the log-log plots ($T_c - T < 10$ K) to be 0.5±0.1. Similar temperature dependence of θ was generally observed for other Sm C or Sm*C adjacent to Sm A.[10]

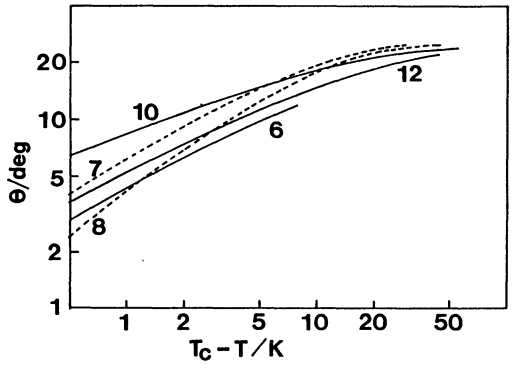

Fig. 4. Temperature dependence of tilt angles. T_c is Sm*C-Sm A transition temperature.

Selective reflection wavelengths were also measured to estimate helical pitches from the relation, $\lambda = \bar{n}p$, where λ is the wavelength, $\bar{n}$ is the average refractive index and p is the pitch. They are located in the IR region, while those of the series I were in the wavelengths of visible light.[11] Furthermore, they are less dependent on the chain lengths, especially in the lower temperature range (<100 °C), as shown in Fig. 5, than in the case of the series I with a remarkable

Table 3. Bond Lengths (Å) and Angles (°) of II-7 and II-8

Atom	II-7	II-8	Atom	II-7	II-8
O(1)-C(13)	1.209(9)	1.182(18)	C(1)-C(2)-C(3)	120.5(5)	116.9(12)
O(2)-C(13)	1.337(8)	1.352(16)	C(2)-C(3)-C(4)	120.7(5)	123.9(12)
O(2)-C(14)	1.406(8)	1.407(13)	C(3)-C(4)-C(5)	118.4(5)	116.3(11)
O(3)-C(1)	1.363(7)	1.363(15)	C(3)-C(4)-C(7)	120.4(5)	120.6(10)
O(3)-C(31)	1.417(10)	1.457(20)	C(5)-C(4)-C(7)	121.2(5)	123.0(10)
C(1)-C(2)	1.381(8)	1.380(17)	C(4)-C(5)-C(6)	120.4(5)	121.1(11)
C(1)-C(6)	1.395(8)	1.384(17)	C(1)-C(6)-C(5)	121.0(5)	119.0(11)
C(2)-C(3)	1.384(8)	1.391(19)	C(4)-C(7)-C(8)	120.6(5)	119.8(11)
C(3)-C(4)	1.386(8)	1.390(17)	C(4)-C(7)-C(12)	121.4(4)	120.5(10)
C(4)-C(5)	1.404(8)	1.408(17)	C(8)-C(7)-C(12)	117.9(5)	119.7(11)
C(4)-C(7)	1.518(7)	1.505(16)	C(7)-C(8)-C(9)	120.8(6)	117.4(11)
C(5)-C(6)	1.363(8)	1.388(18)	C(8)-C(9)-C(10)	120.9(7)	124.2(15)
C(7)-C(8)	1.391(8)	1.383(19)	C(9)-C(10)-C(11)	118.4(6)	117.0(11)
C(7)-C(12)	1.396(7)	1.407(16)	C(9)-C(10)-C(13)	118.3(6)	118.9(11)
C(8)-C(9)	1.378(10)	1.394(23)	C(11)-C(10)-C(13)	123.2(5)	124.2(11)
C(9)-C(10)	1.389(10)	1.388(20)	C(10)-C(11)-C(12)	120.6(5)	120.7(11)
C(10)-C(11)	1.392(8)	1.385(16)	C(7)-C(12)-C(11)	121.2(5)	120.7(11)
C(10)-C(13)	1.470(9)	1.453(17)	O(1)-C(13)-O(2)	122.1(7)	120.5(13)
C(11)-C(12)	1.371(8)	1.385(18)	O(1)-C(13)-C(10)	124.1(6)	126.4(13)
C(14)-C(15)	1.382(9)	1.384(16)	O(2)-C(13)-C(10)	113.7(6)	112.9(11)
C(14)-C(19)	1.379(8)	1.393(15)	O(2)-C(14)-C(15)	120.5(5)	116.2(9)
C(15)-C(16)	1.381(9)	1.393(17)	O(2)-C(14)-C(19)	119.2(5)	123.6(9)
C(16)-C(17)	1.389(9)	1.381(18)	C(15)-C(14)-C(19)	120.3(6)	120.1(10)
C(17)-C(18)	1.386(9)	1.389(17)	C(14)-C(15)-C(16)	120.0(6)	119.7(11)
C(17)-C(21)	1.520(13)	1.501(21)	C(15)-C(16)-C(17)	120.2(6)	120.2(12)
C(18)-C(19)	1.390(9)	1.383(16)	C(16)-C(17)-(18)	119.6(6)	120.1(11)
C(21)-C(22)	1.505(16)	1.525(23)	C(16)-C(17)-C(21)	119.0(7)	124.8(12)
C(22)-C(23)	1.513(21)	1.528(28)	C(18)-C(17)-C(21)	121.4(7)	115.1(12)
C(22)-C(25)	1.499(41)	1.496(31)	C(17)-C(18)-C(19)	120.1(6)	119.7(11)
C(23)-C(24)	1.498(40)	1.489(45)	C(14)-C(19)-C(18)	119.8(6)	120.2(10)
C(31)-C(32)	1.521(11)	1.462(23)	C(17)-C(21)-C(22)	116.6(9)	115.2(13)
C(32)-C(33)	1.520(13)	1.522(22)	C(21)-C(22)-C(23)	111.1(11)	109.6(15)
C(33)-C(34)	1.517(14)	1.499(23)	C(21)-C(22)-C(25)	104.0(17)	109.9(15)
C(34)-C(35)	1.516(14)	1.516(26)	C(23)-C(22)-C(25)	106.2(18)	109.8(17)
C(35)-C(36)	1.524(17)	1.515(35)	C(22)-C(23)-C(24)	115.2(18)	110.3(22)
C(36)-C(37)	1.508(23)	1.499(58)	O(3)-C(31)-C(32)	107.6(6)	107.1(13)
C(37)-C(38)	—	1.513(65)	C(31)-C(32)-C(33)	109.8(7)	110.3(13)
C(22)-C(25′)	1.73(12)	—	C(32)-C(33)-C(34)	114.8(8)	115.7(13)
C(13)-O(2)-C(14)	117.3(5)	116.8(9)	C(33)-C(34)-C(35)	114.9(8)	112.5(14)
C(1)-O(3)-C(31)	119.1(5)	119.9(11)	C(34)-C(35)-C(36)	109.9(9)	109.9(17)
O(3)-C(1)-C(2)	125.9(5)	124.2(11)	C(35)-C(36)-C(37)	112.4(12)	112.7(27)
O(3)-C(1)-C(6)	115.3(5)	113.6(10)	C(36)-C(37)-C(38)	—	111.7(37)
C(2)-C(1)-C(6)	118.8(5)	122.2(11)	C(21)-C(22)-C(25′)	121(7)	—

Table 4. Torsion Angles (°)

	II-7	II-8
Phenyl ring		
Ring(C 1—C 6)-Ring(C 7—C12)	4.1	6.7
Ring(C 7—C12)-Ring(C14—C19)	68.2	69.4
Alkyl chain		
O(3)-C(31)-C(32)-C(33)	190.4	180.1
C(31)-C(32)-C(33)-C(34)	194.3	179.9
C(32)-C(33)-C(34)-C(35)	−55.2	66.5
C(33)-C(34)-C(35)-C(36)	187.3	164.8
C(34)-C(35)-C(36)-C(37)	179.7	151.9
C(35)-C(36)-C(37)-C(38)	—	194.7

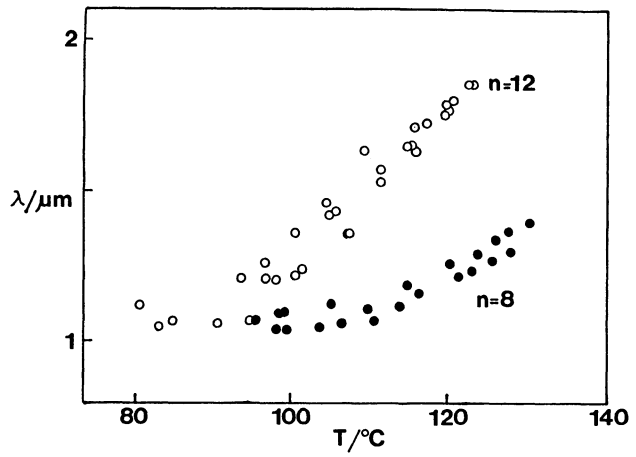

Fig. 5. Temperature dependence of selective reflection wavelengths of II-8 and II-12.

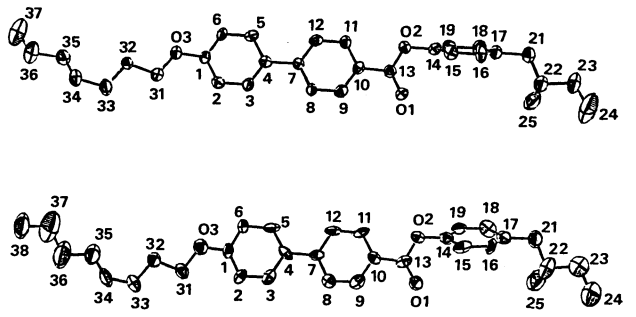

Fig. 6. ORTEP views of the molecules of II-7 (upper) and II-8 (lower) with 50% probability thermal ellipsoids. Only one of the two conformers of the disordered part is shown for simplicity.

dependence on the chain length.[4] A pitch increases with increase in temperature near the Sm*C-Sm A transition point and the increase is more rapid for a longer member.

Molecular Conformations in the Crystals. The ORTEP drawings[12] of the molecular conformations with numbering schemes are shown in Fig. 6. All the bond lengths and angles are compatible with those found in other mesogens,[1] as shown in Table 3. All the phenyl rings are planar within the experimental error. Table 4 shows torsion angles. The conformations of II-7 and II-8 are very similar to each other:

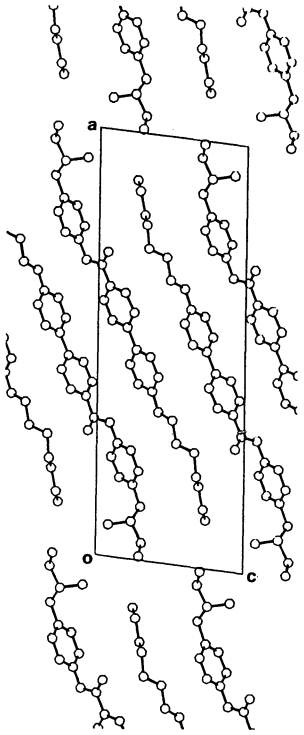

Fig. 7. Crystal structure of 11-7 viewed along the b axis.

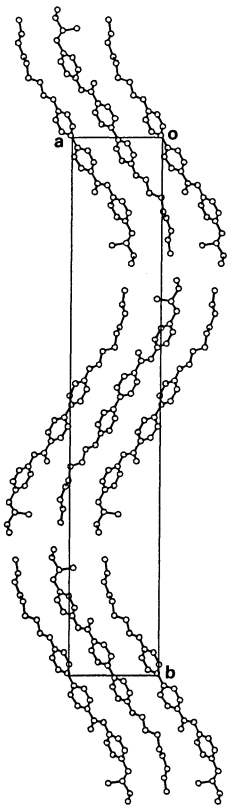

Fig. 8. Crystal structure of II-8 viewed along the c axis.

approximately coplanar biphenyl moieties and paraffin chains with the twisted C(32)-C(33)-C(34)-C(35) moieties. The twisted chains result in straight rod-

shaped molecules as a whole. For II-7, the C(25) atom is slightly disordered.

Crystal Packing. Figures 7 and 8 show the crystal structures of II-7 and II-8, respectively. Both crystals have distinct layer structures, whose layer planes are parallel to (100) plane (II-7) and (010) plane (II-8). Such layer structures were also observed in other smectogens. Structures within a layer are also strikingly similar, composed of the rod-shaped molecules described above. Intermolecular relation except the "extra" C(38) is almost the same in spite of the difference in the chain length. The whole molecule including a normal paraffin chain relates to the lateral packing in the layer, in contrast to the case of the series I, in which paraffin chains have contacts with each other between layers.[1] These facts suggest that interaction between core parts is more dominant in the crystal packing of the series II than that of the series I. This results in a large extent of molecular overlapping within a layer, leading to distinct layer structures with a small tilt angle (30°).

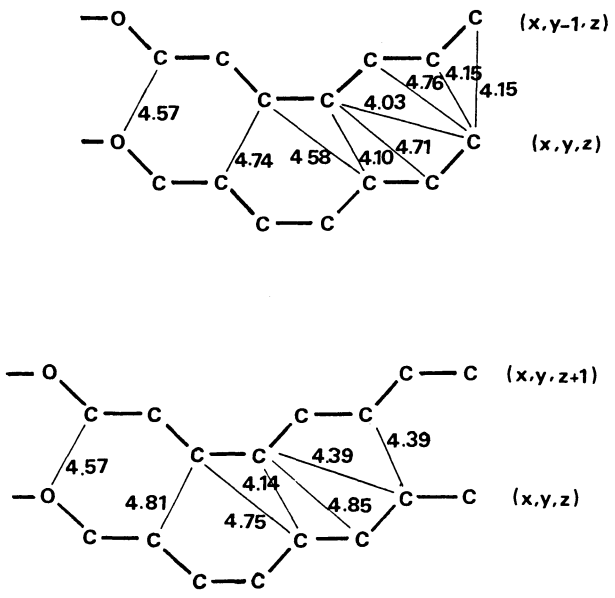

Fig. 9. Interchain distances (Å) of II-7 (upper) and II-8 (lower). Symmetry codes are shown in parentheses.

Figure 9 shows interchain distances. The chains make contacts each other only within a layer. Most of the distances are remarkably longer than those of interlayer chain contacts in the series I. This also suggests that interaction between cores is dominant in the series II.

The phenyl rings of adjacent molecules have nonparallel contacts as found in the I crystals. The angles between the mean planes are 67° (II-7) and 66° (II-8).

The II-7 crystal has a uniform direction of molecular tilt throughout layers, while in the II-8 crystal molecules have two opposite tilt direction alternately from layer to layer. This difference is regarded as induced by a small interlayer interaction in these crystals, since the two crystals of the series I with close contacts of paraffin chains between layers showed similar modes of layer stacking to each other. Both arrangements are known as polytypes for normal long-chain compounds and energy difference is reported to be very small; an alternate arrangement was evaluated to be more stable than a uniform one by 0.73 kJ mol^{-1} for octadecanoic acid.[14] In the present case, less penetration of chains into an adjacent layer in II-8 means less interlayer interaction than in II-7, corresponding to the lower melting point as described above.

Discussion

A relationship between the mesophase structures and the crystal structures are shown schematically in Fig. 10. The tilt angle in the crystals (30°) is closely related to that (22—25°) at the lowest temperature in Sm*C. This suggests that molecular rearrangements at the cryst.-Sm*C transition point are not large in spite of the large enthalpy of transition, as in the case of the series I. Nonparallel contacts of the phenyl rings would enable the molecules to begin to rotate at the melting points, leading to the direct transition to Sm*C. The transition is supposed to be caused by loosening of the core-core interaction, because the contacts of normal alkyl chains within a layer are

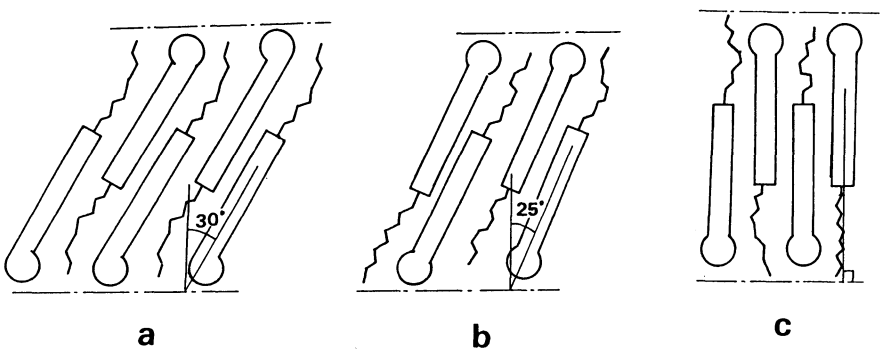

Fig. 10. Schematic diagrams of the structures of the crystal (a), Sm*C (b), and Sm A (c).

loose enough in the crystalline states. On the other hand, molecular overlapping in the layer is much larger than that in the series I. Besides, the interlayer aggregation of the paraffin chains observed in the series I, which was proposed to keep the tilt angles constant, is not found in the series II. Therefore, the molecules gradually change the tilt angles to zero with keeping layer structures; i.e. Sm*C transforms to Sm A. Paraffin chains have a twisted form even in the crystalline states. This corresponds to the small change of their contribution to the layer thickness throughout the Sm*C and Sm A phases, while in the series I, the large change of the paraffin chain organization in the Sm*C was interpreted as the melting process of the chains which are regularly organized in the crystalline states.

Interlayer interaction in the series II is found to be much less than in the series I. This fact seems to be related to the fact that helical pitches in the series II are larger than those in the series I and they are less dependent on the chain lengths. However, further investigation for more variety of compounds would be required to confirm the relationship between the helical pitch and the interlayer interaction.

It is concluded that the mesophase behavior of Sm*C between crystalline and Sm A phases is well interpreted by the intermolecular interaction revealed in the crystal sturctures, as in the case of Sm*C between crystalline and cholesteric phases.

The authors express their thanks to Professor Naoyuki Koide of Science University of Tokyo for DSC measurements and BDH Chemicals Ltd. for supplying the chiral phenol. This work was partially supported by a Grant-in-Aid for Scientific Research No. 60540280 from the Ministry of Education, Science and Culture.

References

1) K. Hori and Y. Ohashi, *Bull. Chem. Soc. Jpn.*, **61**, 3859 (1988).

2) J. W. Goodby and T. M. Leslie, *Mol. Cryst. Liq. Cryst.*, **110**, 175 (1984).

3) G. W. Gray and J. W. Goodby, "Smectic Liquid Crystals," Leonard Hill, Glasgow (1984), p. 54.

4) K. Hori, *Mol. Cryst. Liq. Cryst.*, **123**, 321 (1985).

5) P. Main, S. E. Hull, L. Lessinger, G. Germain, J.-P. Declercq, and M. M. Woolfson, MULTAN78. A System of Computor Programs for the Automatic Solution of X-ray Diffraction Data. Univs. of York, England and Louvain, Belgium (1978).

6) G. M. Sheldrick, SHELX76. A Program for Crystal Structure Determination. Univ. of Cambridge (1976).

7) "International Tables for X-ray Crystallography," Birmingham, Kynoch Press (1974), Vol. IV.

8) The tables for the anisotropic temperature factors for non-hydrogen atoms, the tables for the atomic parameters for the hydrogen atoms and the F_o-F_c list are deposited as Document No. 8875 at the Office of the Editor of the Bulletin of the Chemical Society of Japan.

9) G. W. Gray and J. W. Goodby, *Mol. Cryst. Liq. Cryst.*, **37**, 157 (1976).

10) J. Doucet, A.-M. Levelut, and M. Lanbert, *Mol. Cryst. Liq. Cryst.*, **24**, 317 (1973); Ph. Martino-Lagarde, R. Duke, and G. Durand, *Mol. Cryst. Liq. Cryst.*, **75**, 249 (1981).

11) G. W. Gray and D. G. McDonnell, *Mol. Cryst. Liq. Cryst.* **37**, 189 (1976).

12) C. Johnson, ORTEP. Report ORNL-3794, Oak Ridge National Laboratory, Tennessee (1965).

13) P. Mandal, S. Paul, H. Shenk, and K. Goubitz, *Mol. Cryst. Liq. Cryst.*, **135**, 35 (1986).

14) M. Kobayashi, T. Kobayashi, Y. Cho, and F. Kaneko, *Makromol. Chem., Macromol. Symp.*, **5**, 1 (1986).